International Journal of Nanomedicine

Dovepress
open access to scientific and medical research

Open Access Full Text Article

ORIGINAL RESEARCH

Sustained release of VH and rhBMP-2 from nanoporous magnesium–zinc–silicon xerogels for osteomyelitis treatment and bone repair

This article was published in the following Dove Press journal:
International Journal of Nanomedicine
22 June 2015
Number of times this article has been viewed

Fengqian Li[1,*]
Wen Wu[2,*]
Li Xiang[1]
Gan Weng[1]
Hua Hong[3]
Hong Jiang[4]
Jun Qian[3]

[1]Department of Pharmacy, Shanghai Xuhui Dahua Hospital, [2]Department of Orthopaedics, Ninth People's Hospital, School of Medicine, Shanghai Jiaotong University, [3]Key Laboratory for Ultrafine Materials of Ministry of Education, East China University of Science and Technology, [4]School of Materials Science and Engineering, University of Shanghai for Science and Technology, Shanghai, People's Republic of China

*Co-first authors contributed equally to this work

Abstract: Nanoporous magnesium–zinc–silicon (n-MZS) xerogels with a pore size of ~4 nm, a surface area of 718 cm^2/g, and a pore volume of 1.24 cm^3/g were synthesized by a sol–gel method. The n-MZS xerogels had high capacity to load vancomycin hydrochloride (VH) and human bone morphogenetic protein-2 (rhBMP-2), after soaking in phosphate buffered saline (PBS) for 24 hours (1.5 and 0.8 mg/g, respectively). Moreover, the n-MZS xerogels exhibited the sustained release of VH and rhBMP-2 as compared with magnesium–zinc–silicon (MZS) xerogels without nanopores (showing a burst release). The VH/rhBMP-2/n-MZS system not only exhibited a good antibacterial property but also promoted the MG63 cell proliferation and differentiation demonstrating good bactericidal activity and cytocompatibility. The results suggested that n-MZS with larger surface area and high pore volume might be a promising carrier for loading and sustained release of VH and rhBMP-2. Hence, the VH/rhBMP-2/n-MZS system might be one of the promising biomaterials for osteomyelitis treatment and bone repair.

Keywords: nanoporous xerogels, sustained release, drugs, osteomyelitis, bone regeneration, bactericidal activity, cytocompatibility

Introduction

Nanoporous materials have received increasing attention due to their potential applications in catalysis, separation, sensing, drug delivery, and enzyme immobilization.[1–6] To date, some studies have reported the design of drug-delivery systems based on the nanoporous materials for loading therapeutic molecules, such as chemical drugs, peptides, and proteins.[7,8] As an effective vector-delivering therapeutic molecules, the nanoporous materials with the pore size of a few nanometers have high capacity to encapsulate large amounts of drugs/biomolecules.[9]

Recently, the use of nanoporous materials for bone repair has been proposed, and the tunable pore size, large surface area, and high pore volume might allow them to load osteogenic agents and promote new bone regeneration.[10,11] Human bone morphogenetic protein-2 (rhBMP-2) with strong bone-inducing activity is considered to play important roles in bone regeneration.[12,13] However, the activity of rhBMP-2 is deteriorated by its short in vivo half-life, that is, rhBMP-2 can be quickly diluted and metabolized.[14] Therefore, a suitable carrier is required for preventing rhBMP-2 from degradation and preserving its activity in bone defects.

Osteomyelitis, a type of bone infection, is usually caused by bacteria.[15] Some studies indicated that maintaining a sufficient antibiotic concentration at the site of bone infection was the key to a successful treatment of osteomyelitis. Thus, local antibiotic administration has been developed to improve the treatment effects.[16–18] In order to achieve a sustained antibiotic concentration at the site of bone infection, different kinds

Correspondence: Hua Hong; Jun Qian
Key Laboratory for Ultrafine Materials of Ministry of Education, East China University of Science and Technology, 130 Meilong Road, Shanghai 200237, People's Republic of China
Tel +86 21 6453 5555
Email biomaterbone@163.com; qianjun@ecust.edu.cn

of local delivery systems such as bone cements, bioceramics, bioglasses, and biopolymer coatings have been developed to load antibiotics.[19–22] Vancomycin hydrochloride (VH) is one of the most effective antibiotics for treating osteomyelitis. However, traditional therapy including injections and oral administration has some drawbacks.[23] Therefore, in this study, nanoporous magnesium–zinc–silicon (n-MZS) xerogels were prepared, and the loading and release of VH and rhBMP-2 were investigated. Moreover, the effects of n-MZS xerogels loading VH and rhBMP-2 on antibiosis and MG63 cell behavior were also evaluated in vitro.

Materials and methods

Preparation and characterization of n-MZS xerogels

The n-MZS xerogels were prepared using the template-induced sol–gel method.[4–6] The non-ionic block copolymer $EO_{20}PO_{70}EO_{20}$ (Pluronic P123, molecular weight =5,800, Sigma-Aldrich, St Louis, MO, USA) was used as the template agent. In brief, 4.8 g of P123 was dissolved in 480 mL of 0.1 M HCl aqueous solution at 50°C to obtain a white emulsion. Tetraethyl orthosilicon (Ling Feng Chemical Reagent Co., Ltd, Shanghai, People's Republic of China), $Ca(NO_3)_2{\cdot}4H_2O$ (3.75 g), and $Zn(NO_3)_2{\cdot}6H_2O$ (0.75 g) were then added successively into the aforementioned suspension and stirred vigorously for 12 hours. After that, the reaction system was adjusted to pH 9 using ammonia, and placed in an oven at 120°C for 24 hours. The white precipitate was collected by filtration, washed with ethanol and deionized water, and then dried in an oven at 50°C for 24 hours. The final products were obtained after calcination at 600°C for 5 hours (a ramping rate of 5°C min^{-1}). Magnesium–zinc–silicon (MZS) xerogels without nanopores were prepared as a control using the same procedure but without the addition of P123.

The surface morphology and microstructure of the n-MZS xerogels were characterized using high-resolution transmission electron microscopy (HR-TEM, JEM-1400; JEOL, Tokyo, Japan) and scanning electron microscopy (SEM, JSM-6360LV; JEOL). The specific surface area, pore size, pore volume, and pore size distribution were determined by using Brunauere–Emmette–Teller (BET) and Barrete–Joynere–Halenda analyses.

VH loading on n-MZS xerogels

The VH obtained from Shanghai Eighth People Hospital was dissolved in phosphate buffered saline (PBS, pH 7.4) solution (10 mg/mL). After the VH solution was diluted into different concentrations (0.4, 0.2, 0.1, 0.08, 0.06, 0.04, 0.02, and 0.01 mg/mL), the standard curve of VH was made by using an ultraviolet absorption spectrometer (at 280 nm).

The VH solution was prepared by dissolving 2 mg of VH in 20 mL of H_2O in a tube. Then, 1 g of n-MZS xerogels (MZS as a control) was added into the tube. The tube was placed in a refrigerated shaker with a speed of 100 rpm at 37°C. The solution was centrifuged after 0, 0.5, 1, 2, 4, 8, 12, 24, and 48 hours. The supernatant (0.5 mL) was taken out from the tube and its absorbance was measured at 280 nm. PBS solution of 0.5 mL was added into the tube to maintain the constant volume of 20 mL. The VH concentration was determined using the standard curve. The drug loading efficacy was measured as $EV = (m_1/m_2) \times 100\%$, where EV is the drug loading efficacy and m_1 and m_2 are drug loading mass on the material and total drug mass, respectively.

rhBMP-2 loading on n-MZS xerogels

The 1 mg/mL rhBMP-2 solution was prepared by dissolving rhBMP-2 (Shanghai Rebone Biomaterials Co. Ltd, Shanghai, People's Republic of China) into 1 mL glacial acetic acid (0.2%). After the rhBMP-2 solution was diluted into different concentrations (0.5, 0.4, 0.3, 0.2, and 0.1 mg/mL), the standard curve of rhBMP-2 was made by using an ultraviolet absorption spectrometer (at 450 nm).

In all, 1 g n-MZS (MZS as a control) was then added into 20 mL rhBMP-2 solution (rhBMP-2=1 mg). The solution was placed in a refrigerated shaker with a speed of 100 rpm at 37°C. The solution was centrifuged after 0, 0.5, 1, 2, 4, 8, 12, 24, and 48 hours. The supernatant (0.5 mL) was collected and its absorbance was measured at 450 nm. In all, 0.5 mL PBS solution was added to maintain the sample volume unchanged. The protein concentration was determined using the standard curve. The protein loading efficacy was measured as $EP = (m_1/m_2) \times 100\%$, where EP is the protein loading efficacy, and m_1 and m_2 are the protein loading mass on the material and total protein mass, respectively.

VH and rhBMP-2 release from n-MZS xerogels

VH release from n-MZS xerogels

In all, 1 g VH/n-MZS (VH/MZS as a control) was immersed in 20 mL of PBS at 37°C with shaking at 100 rpm. At each time point (0, 1, 2, 4, 8, 12, 24, 48, 72, 120, 168, 240, 288, and 336 hours), 0.5 mL supernatant solution was extracted for VH measurement by using an ultraviolet absorption spectrometer at 280 nm, and the same volume of fresh PBS was added to the release solution. The cumulative VH release

amount ratio (the ratio of release amount to the total VH amount) was calculated by the concentration of PBS supernatant at each time point using the VH standard curve. In this experiment, each group had three parallel samples and the results were expressed as mean ± standard deviation (SD).

rhBMP-2 release from n-MZS xerogels

In all, 1 g rhBMP-2/n-MZS (rhBMP-2/MZS as a control) was placed in the 20 mL PBS solution (pH 7.4). The suspension was incubated in a refrigerated shaker with a speed of 80 rpm at 37°C. The 0.5 mL supernatant was then extracted from the solution. After that, the same amount of fresh PBS was added in to the solution. The rhBMP-2 quantity in the supernatant was determined using the Bradford protein assay method. The released quantity of rhBMP-2 was measured at 0, 1, 2, 4, 8, 12, 24, 48, 72, 120, 168, 240, 288, and 336 hours, and the absorbance of supernatant was measured at 450 nm. The cumulative rhBMP-2 release was calculated by the concentration of supernatant at each time point using the rhBMP-2 standard curve. The measurement was performed three times and the results were presented as mean ± SD.

VH and rhBMP-2 release from n-MZS xerogels

In all, 1 g VH/rhBMP-2/n-MZS was prepared by mixing 0.5 g VH/n-MZS and 0.5 g rhBMP-2/n-MZS homogeneously. Then, the VH/rhBMP-2/n-MZS system was placed in a centrifuge tube (20 mL). Subsequently, 10 mL PBS solution (pH 7.4) was added into the tube. The suspension was incubated in a refrigerated shaker with a speed of 80 rpm at 37°C. At 0, 1, 2, 4, 8, 12, 24, 48, 72, 120, 168, 240, 288, and 336 hours, the supernatant (0.5 mL) was collected from the solution for absorbance measurement, and meanwhile, 0.5 mL fresh PBS solution was added into the solution. VH quantity and rhBMP-2 quantity in that were determined as described earlier. The release curve was made by plotting the release percentage of VH and rhBMP-2 (the ratio of release amount to the total VH and rhBMP-2 amount), respectively, against the time. In this experiment, all values presented were the average of three tests in each group, and the results were expressed as mean ± SD.

In vitro bacterial inhibition test

Staphylococcus aureus (ATCC 25923, provided by Guan Yong's group) was used in this study. Coagulase-negative *Staphylococcus* strain was cultured on Trypticase soy agar (TSA; BD Biosciences, Franklin Lakes, NJ, USA) medium at 37°C overnight. The culture was sub-cultured into the required amount for 24 hours. The single strain was cultured at 37°C for 12 hours in 10 mL of BBL Trypticase soy broth (TSB).

Single bacterial colony was used to inoculate the samples. Samples were immersed in 1 mL of TSB (1×10^6 CFUs/mL) in the 48-well plate (Costar3548; Costar, Washington DC, USA) at 37°C for 12, 24, 48, and 72 hours. Samples were collected at different time intervals, gently washed with PBS for three times and placed in glass tubes with 0.5 mL of TSB. The bacteria attached on the samples were dislodged using ultrasonication (B3500S-MT; Branson Ultrasonics Co., Shanghai, People's Republic of China) for 5 minutes at 50 Hz. After serially diluted by 10-fold, 0.1 mL of each suspension was plated onto BBL TSA. The colony-forming units (CFU) were counted after cultured at 37°C for different time periods. Three parallel plates were used for each test sample. The mean numbers of viable bacterial colonies on TSA were calculated. The n-MZS sample without VH was included as a control.

Cell viability and morphology

The MTT assay was used to evaluate the influences of samples (VH/rhBMP-2/n-MZS VH/rhBMP-2/MZS, n-MZS, and MZS) on cell viability. The evaluation was conducted by culturing MG63 cells (Chinese Academy of Sciences, Shanghai, People's Republic of China) on the samples in 96-well plates for 1, 3, and 5 days. The MG63 cells were seeded in 96-well plates by transferring a certain amount of the cells suspension into each well. The samples were subsequently added into the plates at a concentration of 1 mg/mL and cultured with the cells at 37°C in a 5% CO_2 incubator for 1, 3, and 5 days. In brief, 4 mL MTT (Amresco, Solon, OH, USA) solution (5 mg/mL) was added into each plate and incubated at 37°C for 4 hours. The culture medium was extracted, and the solid residues were washed twice with 150 µL PBS. Thereafter, PBS was replaced with an equal amount (150 µL) of dimethyl sulfoxide (Sigma-Adrich, St Louis, MO, USA). The plates were vibrated for 15 minutes to dissolve formazan. Finally, the optical density (OD) was measured at 490 nm using an ELX Ultra Microplate Reader (Bio-tek, Winooski, VT, USA).

The morphology of the MG63 cells was examined by visualizing the filamentous actin of the cytoskeleton using a confocal laser scanning microscopy (Leica TCS SP2; Leica Microsystems, Heidelberg, Germany). Prior to the microscopic observation, the samples were pressed into disks (Φ 12×2 mm), and 40 µL rhBMP-2 solution with a concentration of 0.5 mg/mL was added dropwise to the specimens. The samples were then placed in 24 wells, and the MG63 cells were seeded on the samples at a density of 5.0×10^4

cells/well. According to the protocol, the cells were fixed with 2.5% glutaraldehyde for 15 minutes and permeabilized with 0.1% Triton X-100 in PBS for another 15 minutes. After washing with PBS for three times, the cells were incubated with FITC-Phalloidin (Abcam, Sigma-Aldrich) for 1 hour and then counterstained with DAPI (Molecular Probe; Sigma-Aldrich) to observe the nucleus after 10 minutes. The cell morphologies were visualized using confocal laser scanning microscopy.

Alkaline phosphatase activity

The alkaline phosphatase (ALP) activity was measured with the ALP assay in osteogenic medium at 4 and 7 days. Briefly, MG63 cells (2.5×10^4 cells/sample) were seeded on the samples VH/rhBMP-2/n-MZS and VH/rhBMP-2/MZS in 24-well plates and then cultured at 37°C, and 100% humidity atmosphere with 5% CO_2. At each time point, the culture medium was removed from the samples and the cells were washed with PBS. In all, 1 mL Nonidet P-40 (0.2%) was added to each well at room temperature for 1 hour to obtain cell lysate. Then, cells were mixed with 50 µL *p*-nitrophenylphosphate (Sigma) substrate solution (1 mg/mL, pH 9) composed of 0.1 mol/L glycine and 0.5 mmol/L $MgCl_2$ in 1 M diethanolamine buffer, and incubated at 37°C for 15 minutes. In all, 100 µL sodium hydroxide (0.1 M) was added to stop the reaction. Then, the OD value was quantified with a microplate reader (SPECTRAmax 384; Molecular Devices LLC, Sunnyvale, CA, USA) at the wavelength of 405 nm. The ALP activity was expressed as OD value per total protein. The total protein content was determined using the BCA protein assay kits and a series of bovine serum albumin standards.

Statistical analysis

All quantitative data were analyzed with Origin 8.0 (OriginLab Corporation, Wellesley, MA, USA) and expressed as the mean ± SD. Statistical comparisons were carried out using one-way analysis of variance (ANOVA) with the post hoc test.

Results and discussion

TEM and SEM examination

Figure 1A shows the TEM image of morphology and microstructure of the n-MZS xerogels. The n-MZS xerogels possessed a highly ordered porous structure with a pore size of 4 nm. Conversely as shown in the SEM image in Figure 1B, the n-MZS xerogels present regular short rod-like particles without visible pores on the surfaces.

BET analysis

The N_2 adsorption–desorption isotherms and pore diameter distribution of the n-MZS are shown in Figure 2. The n-MZS showed a typical type IV isotherm curve, in which the hysteresis loop was clearly evident, implying a highly consistent pore structure. The BET surface area, pore size, and pore volume of n-MZS were measured to be 718 m^2/g, 4 nm, and 1.24 cm^3/g, respectively. On the contrary, the BET surface area and pore volume of MZS were 84 m^2/g and 0.34 cm^3/g, respectively.

VH and rhBMP-2 loaded on n-MZS xerogels

Figure 3A shows the profile of VH loaded into n-MZS xerogels: after immersed in the PBS solution, the amount of VH adsorbed onto n-MZS xerogels was 1.5 mg/g, three times than that for MZS xerogels 0.5 mg/g.

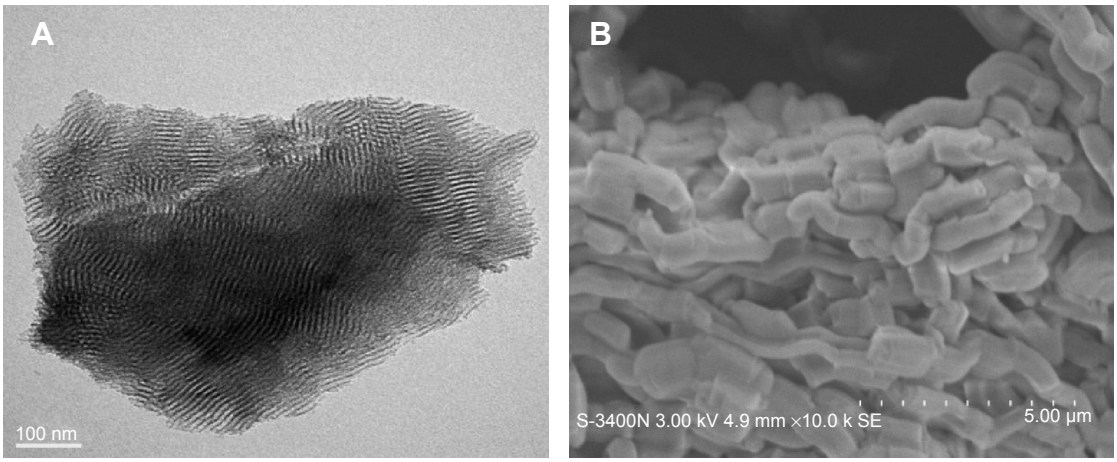

Figure 1 TEM (**A**) and SEM (**B**) images of morphology and microstructure of the n-MZS xerogels.
Abbreviations: n-MZS, anoporous magnesium–zinc–silicon; SE, secondary electron signal types; SEM, scanning electron microscopy; TEM, transmission electron microscopy.

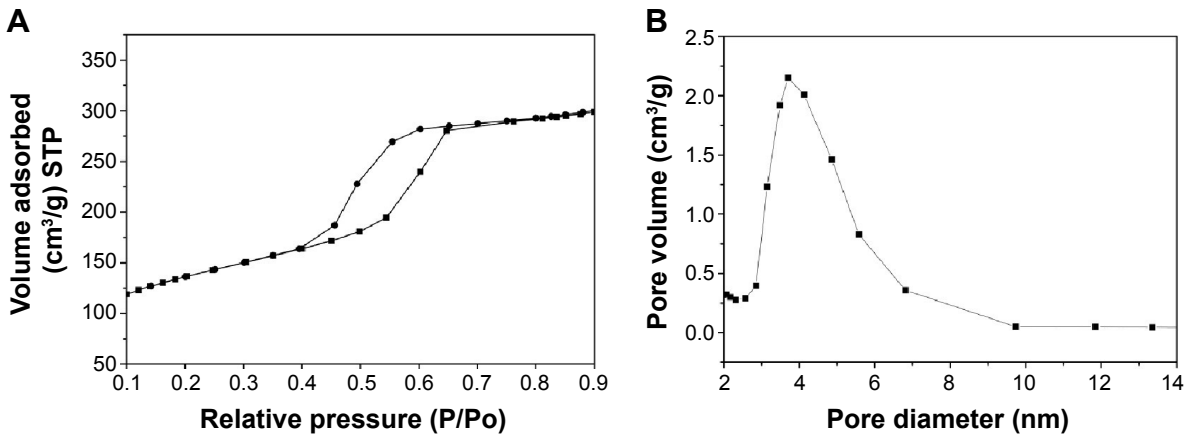

Figure 2 N_2 adsorption–desorption isotherms (**A**) and pore diameter distribution (**B**) of the n-MZS xerogels.
Abbreviations: n-MZS, anoporous magnesium–zinc–silicon; STP, standard temperature and pressure.

Similarly, Figure 3B shows that after 24 hours, the amount of rhBMP-2 adsorbed onto n-MZS xerogels was 0.8 mg/g, significantly higher than that for MZS xerogels (0.3 mg/g). The results indicated that n-MZS xerogels had higher capacity to adsorb VH or rhBMP-2 as compared with MZS xerogels.

Over the past few years, nanoporous materials have shown the potential applications as drug carriers with controlled release kinetic because of the tunable pore size, large surface area, and high pore volume, allowing sufficient incorporation of large quantities of molecules within the nanoporous structure.[24] A study has shown that the surface area and pore volume were two key factors responsible for loading capacity of the drug molecules and subsequent release profiles.[25] In this study, the pore size, specific surface area, and pore volume of n-MZS were of 4 nm, 718 m^2/g, and 1.24 cm^3/g, respectively. In contrast, surface area and pore volume of MZS were 84 m^2/g and 0.34 cm^3/g, respectively. Undoubtedly, the superiority in microstructure of the n-MZS xerogels renders them the higher loading capacity of VH or rhBMP-2 over non-nanoporous MZS xerogels. As a drug-delivery system, the characteristics of nanoporous material such as tunable pore size, large surface area, and high pore volume make it possible to highly efficiently adsorb proteins and/or drug molecules, and provide sustained release from the nanostructured matrices.[26,27]

VH and rhBMP-2 release from n-MZS and MZS xerogels

The cumulative release of VH up to 14 days from n-MZS and MZS xerogels is shown in Figure 4A. Apparently, the MZS xerogels showed a burst release of VH within 10 hours, and

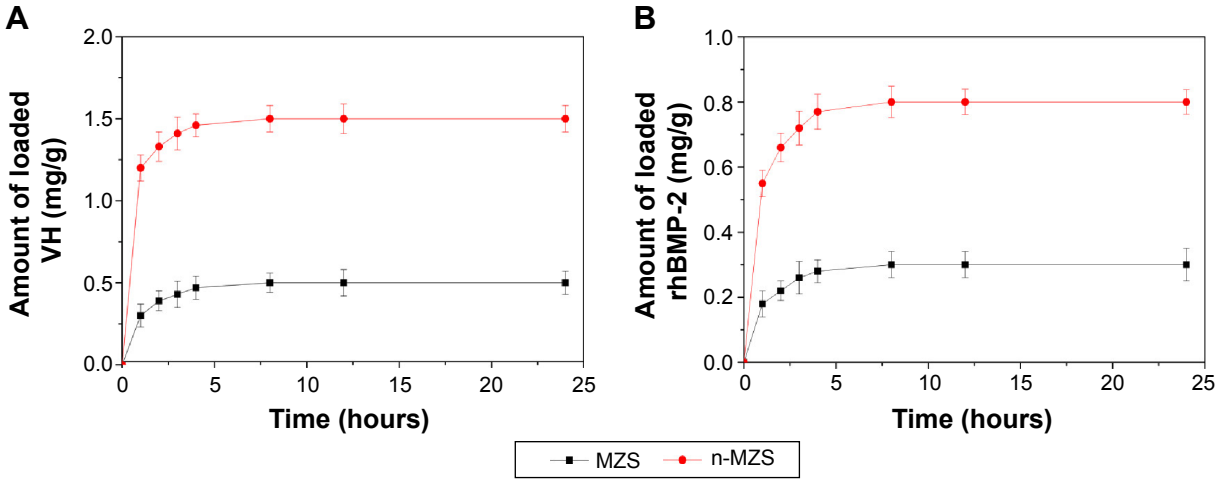

Figure 3 VH (**A**) and rhBMP-2 (**B**) loading on n-MZS and MZS xerogels.
Abbreviations: MZS, magnesium–zinc–silicon; n-MZS, nanoporous magnesium–zinc–silicon; rhBMP-2, human bone morphogenetic protein-2; VH, vancomycin hydrochloride.

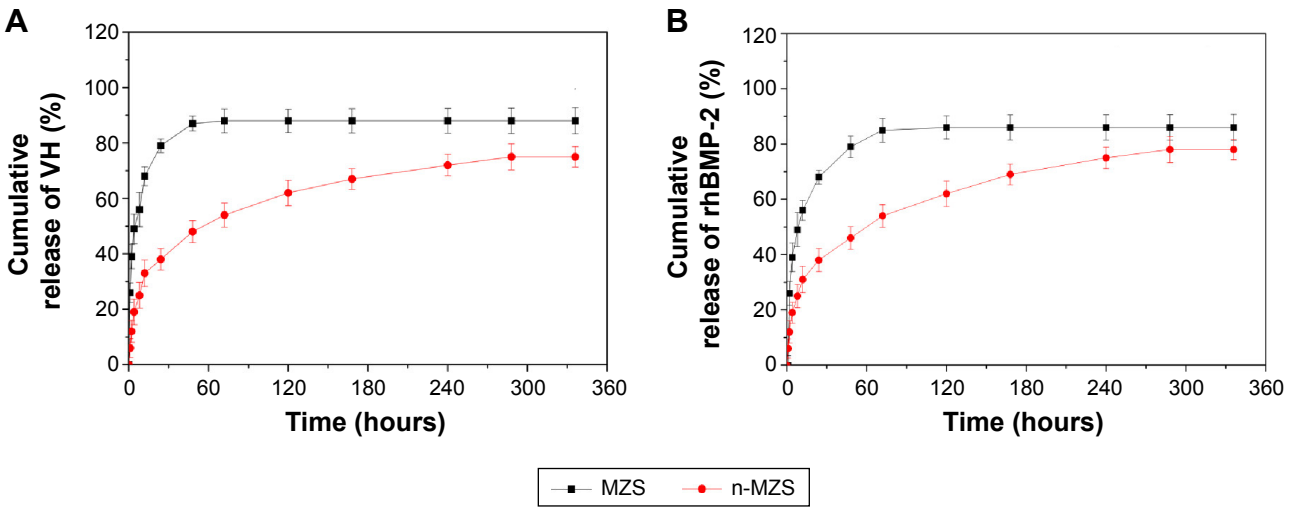

Figure 4 VH (**A**) and rhBMP-2 (**B**) release from n-MZS and MZS xerogels.
Abbreviations: MZS, magnesium–zinc–silicon; n-MZS, nanoporous magnesium–zinc–silicon; rhBMP-2, human bone morphogenetic protein-2; VH, vancomycin hydrochloride.

VH was almost completely released within 2 days. However, the n-MZS xerogels significantly prolonged the release period, and a sustained release was observed in 2 days.

Osteomyelitis remains a serious orthopedic problem in clinics, and antibiotic therapy represents an important step for the treatment of osteomyelitis.[28] A variety of drug-delivery systems were developed for the treatment of osteomyelitis.[29,30] However, long-term systemic administration of antibiotics can be toxic and the antibiosis function might be limited because the drug concentration around the bone infection site was difficult to control.[31] In this study, the VH release experiments showed that 75 wt% VH was released from n-MZS even after 14 days, indicating a clear sustained release of VH from n-MZS. However, more than 85 wt% of VH was released from MZS within 2 days, indicating that the release of VH from MZS was a quick process (burst release) limiting the function of VH at an effective dose in long-term treatment. In a similar manner as demonstrated in Figure 4B more than 84 wt% rhBMP-2 was released from MZS xerogels within 3 days, showing a burst release. Conversely, even after 14 days, only 78 wt% rhBMP-2 was released from n-MZS xerogels. The results indicated that the n-MZS xerogels exhibited sustained release behavior of rhBMP-2 as compared with MZS xerogels.

The rhBMP-2 is the most effective osteoinduction factor and displays potent osteogenesis activity both in vitro and in vivo.[32] In this study, the VH or rhBMP-2 release profiles clearly indicated the sustained release of VH or rhBMP-2 from n-MZS, whereas MZS showed an initial burst release. The large amount of VH or rhBMP-2 could be loaded into n-MZS by a physical adsorption process, which could avoid initial burst release of VH or rhBMP-2. Therefore, n-MZS is a very promising carrier for sustained release of VH or rhBMP-2.

Simultaneous VH and rhBMP-2 release from n-MZS xerogels

In addition to the study of VH or rhBMP-2 loading and release behavior on n-MZS xerogels, more interestingly, in the present study we investigated the co-delivery system, namely, VH/rhBMP-2/n-MZS. Figure 5 shows the profiles of the VH and rhBMP-2 release from the n-MZS xerogels. Both the VH and rhBMP-2 showed a sustained-release behavior from the n-MZS xerogels. The results indicated that n-MZS xerogels exhibited sustained-release behavior of the VH and rhBMP-2, and there were no clear influence on the individual release behaviors of VH and rhBMP-2.

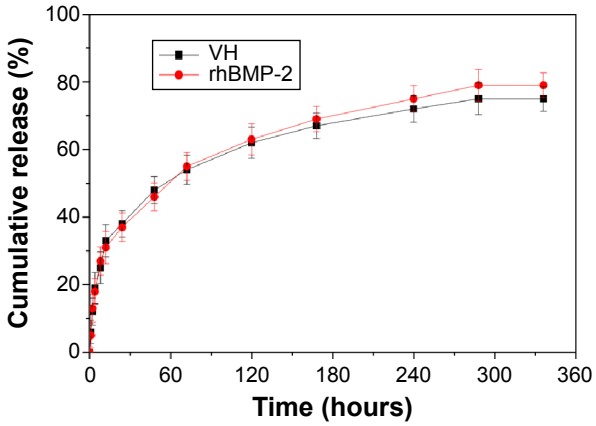

Figure 5 VH and rhBMP-2 release from n-MZS xerogels at different times.
Abbreviations: n-MZS, nanoporous magnesium–zinc–silicon; rhBMP-2, human bone morphogenetic protein-2; VH, vancomycin hydrochloride.

In vitro antibacterial activity

The VH/rhBMP-2/n-MZS system gradually reduced the number of attached *S. aureus* with time (12, 24, 48, and 72 hours) (Figure 6). However, the number of *S. aureus* with the VH/rhBMP-2/MZS gradually was reduced from 12 to 24 hours but increased from 48 to 72 hours. Clearly, the VH/rhBMP-2/n-MZS system had a sustained and effective antibacterial activity, whereas the VH/rhBMP-2/MZS system exhibited the antibacterial property only at the initial time.

The results showed that the VH/rhBMP-2/n-MZS system had good antibacterial properties from 12 to 72 hours. Apparently, the VH/rhBMP-2/n-MZS system, instead of VH/rhBMP-2/MZS, can maintain a sustained and effective antibacterial action for a long time, and prevent the formation of osteomyelitis.

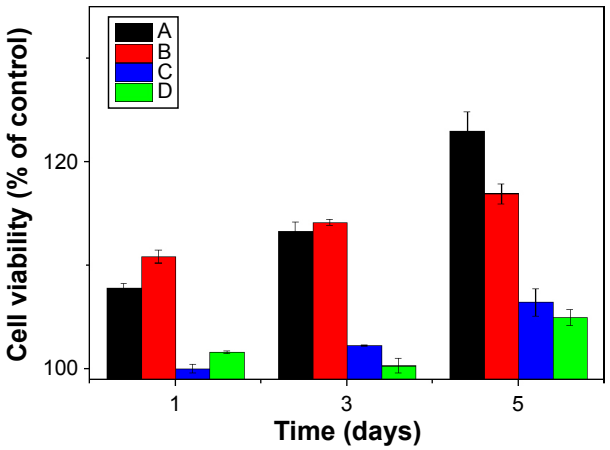

Figure 7 Proliferation of the MG63 cells on the VH/rhBMP-2/n-MZS (**A**) and VH/rhBMP-2/MZS (**B**) systems at 1, 3, and 5 days; n-MZS (**C**); and MZS (**D**) xerogels without VH and rhBMP-2 as controls.
Abbreviations: MZS, magnesium–zinc–silicon; n-MZS, nanoporous magnesium–zinc–silicon; rhBMP-2, human bone morphogenetic protein-2; VH, vancomycin hydrochloride.

Cell proliferation

Cell proliferation of MG63 cells on both the VH/rhBMP-2/n-MZS and VH/rhBMP-2/MZS systems was assessed using the MTT assay. Figure 7 reveals that the OD values of the cells on all the samples increased with time, and the OD values for both VH/rhBMP-2/n-MZS and VH/rhBMP-2/MZS systems were significantly higher than those for n-MZS and MZS without rhBMP-2 at 1, 3, and 5 days. In addition, the OD value for VH/rhBMP-2/MZS was higher than that for the VH/rhBMP-2/n-MZS system at 1 and 3 days. However, the OD value for VH/rhBMP-2/n-MZS was significantly higher than that for the VH/rhBMP-2/MZS system at 5 days.

The cell proliferation of MG63 cells on both VH/rhBMP-2/n-MZS and VH/rhBMP-2/MZS systems was significantly higher than that on n-MZS and MZS without loading rhBMP-2, indicating that MZS loading rhBMP-2 could promote cell proliferation because of rhBMP-2, a growth factor, which has been proved to facilitate cell proliferation and differentiation.[33] In addition, the cell proliferation of MG63 cells on the VH/rhBMP-2/MZS system was higher than the VH/rhBMP-2/n-MZS system at 1 and 3 days which can be attributed to the initial burst release of rhBMP-2 from the VH/rhBMP-2/MZS system stimulating cell growth. However, cell proliferation on the VH/rhBMP-2/n-MZS system was significantly higher than that on the VH/rhBMP-2/MZS system at 5 days, indicating that n-MZS could provide sustained release of rhBMP-2 to promote long-term cell proliferation. The slow release of rhBMP-2 from n-MZS might be due to the retention of a large number of rhBMP-2 by the internal nanopores and preserved its bioactivity. The results indicated that the VH/rhBMP-2/n-MZS system with sustained-release behaviors of rhBMP-2 facilitated cell proliferation continuously.

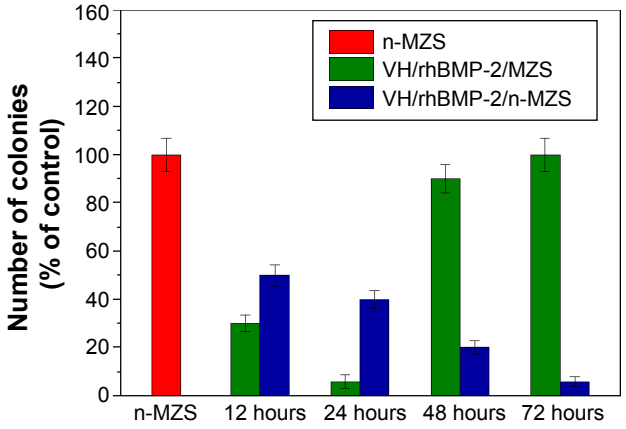

Figure 6 The number of viable bacteria on the sample surfaces was counted and normalized to the counts of n-MZS (control).
Abbreviations: MZS, magnesium–zinc–silicon; n-MZS, nanoporous magnesium–zinc–silicon; rhBMP-2, human bone morphogenetic protein-2; VH, vancomycin hydrochloride.

Cell morphology

The cytoskeletal morphology of the MG63 cells cultured on both the VH/rhBMP-2/n-MZS and VH/rhBMP-2/MZS systems was also studied as demonstrated in Figure 8. The spindle-shaped cells extended and spread well with clearly visible filopodia on both VH/rhBMP-2/n-MZS and VH/rhBMP-2/MZS systems. Moreover, the cell number on the VH/rhBMP-2/n-MZS system was clearly higher than that on the VH/rhBMP-2/MZS system at 5 days. In addition, the cell numbers on both VH/rhBMP-2/n-MZS and VH/rhBMP-2/MZS systems were significantly higher than those on n-MZS and MZS without rhBMP-2 at 5 days. The VH/rhBMP-2/n-MZS system exhibited significant effects on MG63 cell growth among all the groups. The MG63

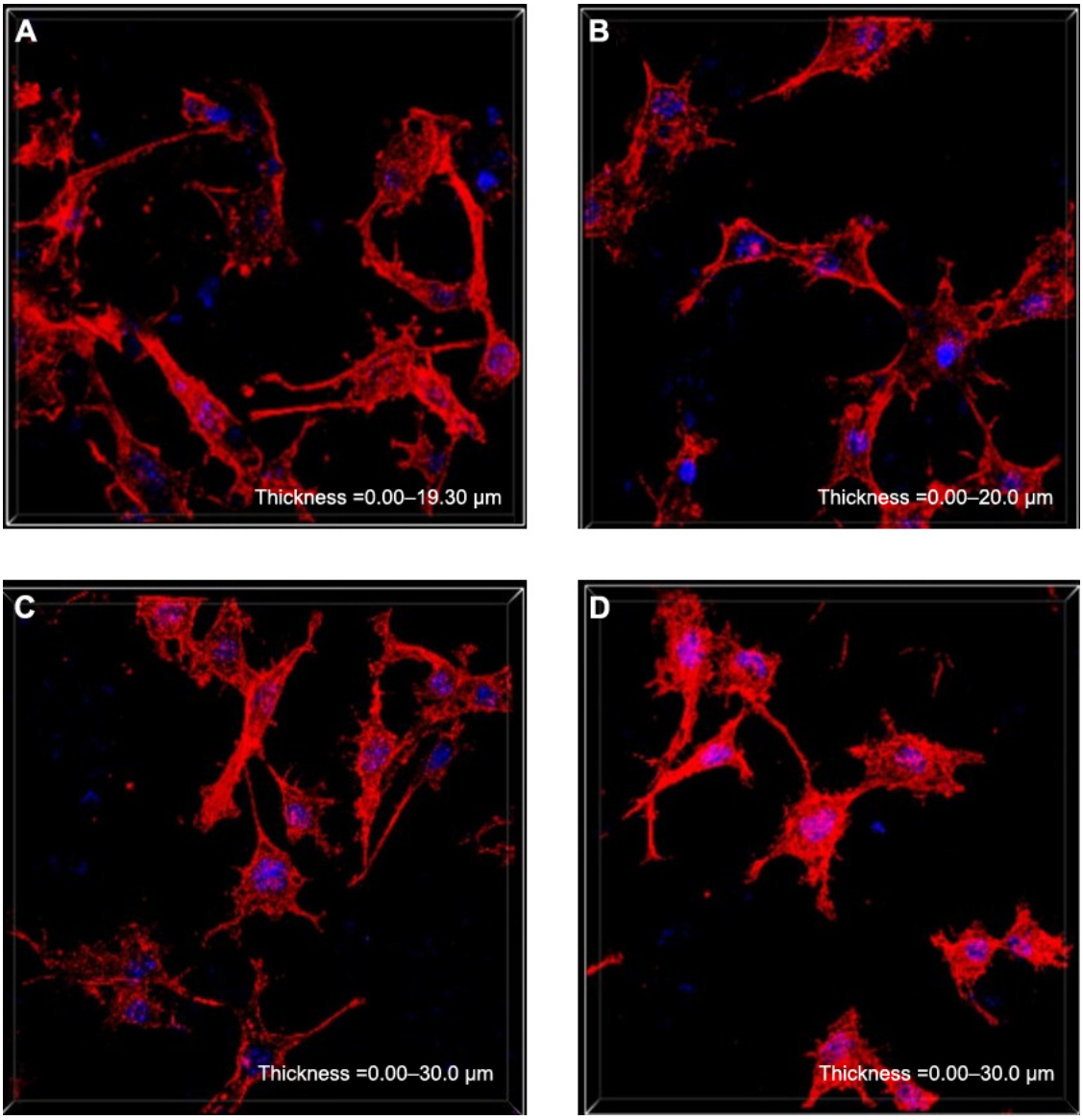

Figure 8 Cytoskeletal morphology of the MG63 cells on the samples for 5 days: VH/rhBMP-2/n-MZS (**A**) and VH/rhBMP-2/MZS (**B**) systems; n-MZS (**C**) and MZS (**D**) xerogels.
Abbreviations: MZS, magnesium–zinc–silicon; n-MZS, nanoporous magnesium–zinc–silicon; rhBMP-2, human bone morphogenetic protein-2; VH, vancomycin hydrochloride.

cells could extend and spread well when cultured on the VH/rhBMP-2/n-MZS, n-MZS, and MZS, indicating that all the samples had good cytocompatibility. More importantly, cell density on the VH/rhBMP-2/n-MZS system was significantly higher than that on the other three samples at 5 days, which could be ascribed to the sustained release of rhBMP-2 from n-MZS. The results strongly suggested that the sustained release of rhBMP-2 from n-MZS exhibited a long-lasting promoting effect on cell proliferation.

ALP activity

The ALP activity of MG63 cells cultured on VH/rhBMP2/n-MZS and VH/rhBMP-2/MZS systems was assessed at 4 and 7 days. Figure 9 depicts that the ALP activity on both VH/rhBMP-2/n-MZS and VH/rhBMP-2/MZS systems was significantly higher than those on n-MZS and MZS without rhBMP-2 at 4 and 7 days. At 4 days, ALP expressed at lower levels, and no significant differences were detected for both VH/rhBMP-2/n-MZS and VH/rhBMP-2/MZS systems. However, the ALP activity of MG63 cells on VH/rhBMP-2/n-MZS was significantly greater than that on the VH/rhBMP-2/MZS system at 7 days.

The ALP activity has been used as an early marker for functionality and differentiation of osteoblasts during in vitro experiments.[34–39] In this study, the ALP activity of MG63 cells on the VH/rhBMP-2/n-MZS exhibited significantly higher levels of expression than that on the VH/rhBMP-2/MZS system at 7 days, indicating that the cells differentiated more quickly

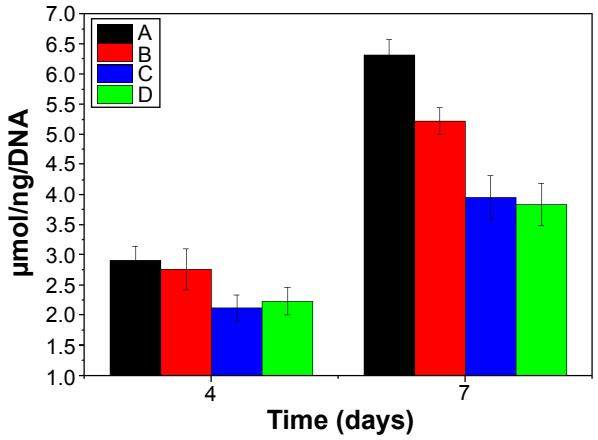

Figure 9 ALP activity of MG63 cells cultured on VH/rhBMP-2/n-MZS (**A**) and VH/rhBMP-2/MZS (**B**) systems at 4 and 7 days, respectively; n-MZS (**C**) and MZS (**D**) xerogels without VH and rhBMP-2 as controls.
Abbreviations: ALP, alkaline phosphatase; MZS, magnesium–zinc–silicon; n-MZS, nanoporous magnesium–zinc–silicon; rhBMP-2, human bone morphogenetic protein-2; VH, vancomycin hydrochloride.

after being cultured on the VH/rhBMP-2/n-MZS than that on the VH/rhBMP-2/MZS system. This increased ALP activity probably resulted from a larger quantity of rhBMP-2 sustained release from n-MZS as compared with MZS. The nanoporous structures of n-MZS with large surface area and high pore volume offered the possibility of adsorbing or entrapping a large number of rhBMP-2 within the nanopores and on the external surface. Such materials improved the diffusion of the rhBMP-2 macromolecules into the nanoporous structures, whereas the MZS only adsorbed rhBMP-2 on its external surface.

Conclusion

The n-MZS xerogels with a pore size of 4 nm, a surface area of 718 cm^2, and a pore volume of 1.24 cm^3/g were synthesized by a sol–gel method. The results showed that the n-MZS xerogels with larger surface area and higher pore volume allowed sufficient loading of VH and rhBMP-2 within the nanoporous structure by a physical adsorption process. In addition, the n-MZS xerogels exhibited the sustained release of VH and rhBMP-2. The sustained release of VH from n-MZS xerogels could continuously inhibit the bactericidal attachment on the samples, showing good bactericidal activity. On the other hand, the sustained release of rhBMP-2 from n-MZS xerogels could promote the proliferation and differentiation of MG63 cells in vitro. It is expected that n-MZS xerogels could be a promising carrier material for loading and sustained release of drugs/biomacromolecules.

Acknowledgments

This study was supported by grants from the National Natural Science Foundation of China (numbers 81172989 and 81301546), the Major Program of Natural Science Foundation of Shanghai, China (13NM1400702), the National Science Fund of Shanghai (number 13ZR1427900), and the Shanghai Education Development Foundation (number Slgl4050).

Disclosure

The authors report no conflicts of interest in this work.

References

1. Qiu HJ, Xu HT, Liu L, Wang Y. Correlation of the structure and applications of dealloyed nanoporous metals in catalysis and energy conversion/storage. *Nanoscale*. 2015;7(2):386–400.
2. Lavoine N, Desloges I, Sillard C, Bras J. Controlled release and long-term antibacterial activity of chlorhexidinedigluconate through the nanoporous network of microfibrillated cellulose. *Cellulose*. 2014;21(6):4429–4442.
3. Zhou H, Wei J, Wu X, et al. The bio-functional role of calcium in mesoporous silica xerogels on the responses of osteoblasts in vitro. *J Mater Sci Mater Med*. 2010;21(7):2175–2185.
4. Zhou H, Wu X, Wei J, et al. Stimulated osteoblastic proliferation by mesoporous silica xerogel with high specific surface area. *J Mater Sci Mater Med*. 2011;22(3):731–739.
5. Wu X, Ye L, Liu K, et al. Antibacterial properties of mesoporous copper-doped silica xerogels. *Biomed Mater*. 2009;4(4):045008.
6. Wu X, Wei J, Lu X, et al. Chemical characteristics and hemostatic performances of ordered mesoporous calcium-doped silica xerogels. *Biomed Mater*. 2010;5(3):035006.
7. Bhunia S, Chatterjee N, Das S, Das Saha K, Bhaumik A. Porous polyurea network showing aggregation induced white light emission, applications as biosensor and scaffold for drug delivery. *ACS Appl Mater Int*. 2014;6(24):22569–22576.
8. Garcia-Gradilla V, Sattayasamitsathit S, Soto F, et al. Ultrasound-propelled nanoporous gold wire for efficient drug loading and release. *Small*. 2014;10(20):4154–4159.
9. Baranowska M, Slota AJ, Eravuchira PJ, et al. Protein attachment to nanoporous anodic alumina for biotechnological applications: influence of pore size, protein size and functionalization path. *Colloids Surf B Biointerfaces*. 2014;122:357–383.
10. Mulvenna RA, Weidman JL, Jing BX, et al. Tunable nanoporous membranes with chemically-tailored pore walls from triblock polymer templates. *J Membr Sci*. 2014;470:246–256.
11. Ma J, Lin HM, Li XF, Bian CH, Xiang D, Qu FY. Synthesis of hierarchical porous bioactive glasses for bone tissue regeneration. *IET Nanobiotechnol*. 2014;8(4):216–221.
12. Jung HD, Jang TS, Wang L, Kim HE, Koh YH, Song J. Novel strategy for mechanically tunable and bioactive metal implants. *Biomaterials*. 2015;37:49–61.
13. Zhou PY, Xia Y, Cheng XS, Wang PF, Xie Y, Xu SG. Enhanced bone tissue regeneration by antibacterial and osteoinductive silica–HACC–zein composite scaffolds loaded with rhBMP-2. *Biomaterials*. 2014;35(38):10033–10045.
14. Gao XQ, Usas A, Tang Y, et al. A comparison of bone regeneration with human mesenchymal stem cells and muscle-derived stem cells and the critical role of BMP. *Biomaterials*. 2014;35(25):6859–6878.
15. Koseki H, Asahara T, Shida T, et al. Clinical and histomorphometrical study on titanium dioxide-coated external fixation pins. *Int J Nanomedicine*. 2013;8:593–599.
16. Emiley PJ, Kendall JL, Bellows JW. Acute hematogenous osteomyelitis of the RIB identified on bedside ultrasound. *J Emerg Med*. 2015;48(1):E15–E17.
17. Na SY, Oh SH, Kim TH, Yoon JA, Lee IS, Lee JH. Sustained release of antibiotic complexed by multivalent ion: in vitro and in vivo study for the treatment of peritonitis. *Int J Pharm*. 2014;476(1–2):213–222.

18. Chow LTC, Wong SKC. Primary osseous inflammatory malignant fibrous histiocytoma masquerading as chronic osteomyelitis. *Orthopedics*. 2014;37(10):E940–E945.
19. Forouzandeh A, Hesaraki S, Zamanian A. The releasing behavior and in vitro osteoinductive evaluations of dexamethasone-loaded porous calcium phosphate cements. *Ceram Int*. 2014;40(1):1081–1091.
20. Chai F, Abdelkarim M, Laurent T, et al. Poly-cyclodextrin functionalized porous bioceramics for local chemotherapy and anticancer bone reconstruction. *J Biomed Mater Res B Appl Biomater*. 2014;102(6):1130–1139.
21. Arcos D, Vallet-Regi M. Sol–gel silica-based biomaterials and bone tissue regeneration. *Acta Biomater*. 2010;6(8):2874–2888.
22. Bhatnagar S, Venuganti VVK. Cancer targeting: responsive polymers for stimuli-sensitive drug delivery. *J Nanosci Nanotechnol*. 2015;15(3):1925–1945.
23. Wang F, Ni B, Zhu ZC, Liu FC, Zhu YZ, Liu J. Intra-discalvancomycin-loaded PLGA microsphere injection for MRSA discitis: an experimental study. *Arch Orthop Trauma Surg*. 2011;131(1):111–119.
24. Matsuyama K, Hayashi N, Yokomizo M, Kato T, Ohara K, Okuyama T. Supercritical carbon dioxide-assisted drug loading and release from biocompatible porous metal-organic frameworks. *J Mater Chem B Mater Biol Med*. 2014;2(43):7551–7558.
25. Duan RX, Xia F, Jiang L. Constructing tunable nanopores and their application in drug delivery. *ACS Nano*. 2013;7(10):8344–8349.
26. Min J, Braatz RD, Hammond PT. Tunable staged release of therapeutics from layer-by-layer coatings with clay interlayer barrier. *Biomaterials*. 2014;35(8):2507–2517.
27. Xue B, Zhang C, Wang YH, et al. A novel controlled-release system for antibacterial enzyme lysostaphin delivery using hydroxyapatite/chitosan composite bone cement. *PLoS One*. 2014;9(12):e113797.
28. Jin GD, Qin H, Cao HL, et al. Synergistic effects of dual Zn/Ag ion implantation in osteogenic activity and antibacterial ability of titanium. *Biomaterials*. 2014;35(27):7699–7713.
29. Chung MF, Chia WT, Liu HY, et al. Inflammation-induced drug release by using a pH-responsive gas-generating hollow-microsphere system for the treatment of osteomyelitis. *Adv Healthc Mater*. 2014;3(11):1854–1861.
30. Uskokovic V, Desai TA. In vitro analysis of nanoparticulate hydroxyapatite/chitosan composites as potential drug delivery platforms for the sustained release of antibiotics in the treatment of osteomyelitis. *J Pharm Sci*. 2014;103(2):567–579.
31. Nardecchia S, Gutierrez MC, Serrano MC, et al. In situ precipitation of amorphous calcium phosphate and ciprofloxacin crystals during the formation of chitosan hydrogels and its application for drug delivery purposes. *Langmuir*. 2012;28(45):15937–15946.
32. Cooley MA, Harikrishnan K, Oppel JA, et al. Fibulin-1 is required for bone formation and Bmp-2-mediated induction of Osterix. *Bone*. 2014;69:30–38.
33. Kim EC, Kim TH, Jung JH, Hong SO, Lee DW. Enhanced osteogenic differentiation of MC3T3-E1 on rhBMP-2-immobilized titanium via click reaction. *Carbohydr Polym*. 2014;103:170–178.
34. Li X, Ma XY, Feng YF, et al. Osseointegration of chitosan coated porous titanium alloy implant by reactive oxygen species-mediated activation of the PI31K/AKT pathway under diabetic conditions. *Biomaterials*. 2015;36:44–54.
35. Wu X, Wang S. Regulating MC3T3-E1 cells on deformable poly (ε-caprolactone) honeycomb films prepared using a surfactant-free breath figure method in a water-miscible solvent. *ACS Appl Mater Interfaces*. 2012;4(9):4966–4975.
36. Wei J, Wu X, Liu C, et al. Fabrication of bioactive scaffold of poly (ε-caprolactone) and nanofiber wollastonite composite. *J Am Ceram Soc*. 2009;92(5):1017–1023.
37. Wu X, Wang S. Integration of photo-crosslinking and breath figures to fabricate biodegradable polymer substrates with tunable pores that regulate cellular behavior. *Polymer*. 2014;55(7):1756–1762.
38. Wu X, Wang S. Biomimetic calcium carbonate concentric microgrooves with tunable widths for promoting MC3T3-E1 cell functions. *Adv Healthc Mater*. 2013;2(2):326–333.
39. Wu X, Wu Z, Su J, et al. Nano-hydroxyapatite promotes self-assembly of honeycomb pores in poly(L-lactide) films through breath-figure method and MC3T3-E1 cell functions. *RSC Adv*. 2014;5(9):6607–6616.